Proc. Natl. Acad. Sci. USA
Vol. 85, pp. 8487–8491, November 1988
Biophysics

Structure of the reaction center from *Rhodobacter sphaeroides* R-26: Protein–cofactor (quinones and Fe^{2+}) interactions*

(bacterial photosynthesis/membrane protein structure/x-ray diffraction)

J. P. ALLEN†, G. FEHER†‡, T. O. YEATES§, H. KOMIYA§, AND D. C. REES§

†University of California at San Diego, La Jolla, CA 92093; and §University of California, Los Angeles, CA 90024

Contributed by G. Feher, August 5, 1988

ABSTRACT **The three-dimensional structure of the reaction center (RC) from *Rhodobacter sphaeroides* has been determined by x-ray diffraction to a resolution of 2.8 Å with an *R* value of 24%. The interactions of the protein with the primary quinone, Q_A, secondary quinone, Q_B, and the nonheme iron are described and compared to those of RCs from *Rhodopseudomonas viridis*. Structural differences between the Q_A and Q_B environments that contribute to the function of the quinones (the electron transfer from Q_A^- to Q_B and the charge recombination of Q_A^-, Q_B^- with the primary donor) are delineated. The protein residues that may be involved in the protonation of Q_B are identified. A pathway for the doubly reduced Q_B to dissociate from the RC is proposed. The interactions between Q_B and the residues that have been changed in herbicide-resistant mutants are described. The environment of the nonheme iron is compared to the environments of metal ions in other proteins.**

The reaction center (RC) is a protein–pigment complex that mediates the primary photochemistry of photosynthetic systems. The RC from *Rhodobacter sphaeroides* R-26 is composed of three protein subunits (L, M, and H) and several cofactors (for a review, see ref. 1). Serving as electron acceptors are the primary quinone Q_A and the secondary quinone Q_B. In *Rb. sphaeroides* both quinones are ubiquinones, whereas in *Rhodopseudomonas viridis* Q_A is a menaquinone and Q_B is a ubiquinone.

The three-dimensional structure of the RC from *Rb. sphaeroides* R-26 has been obtained to a resolution of 2.8 Å (2–4) and an *R* value of 24%. In this paper, we describe the interactions of the protein with the quinones and the nonheme iron. We emphasize structural features that appear to be important in electron and proton transfer. Differences in the interactions of the protein with the quinones in *Rb. sphaeroides* and *Rps. viridis* are described, although a detailed comparison between the Q_B interactions is difficult because of the low occupancy of the Q_B sites in crystals of *Rps. viridis* (5, 6). The interactions with the nonheme iron are found to be very similar for the two bacterial species. The interactions of the protein with the other cofactors as well as the crystallographic procedures have been reported (7). In a subsequent paper (8), the asymmetries of the two branches of the cofactors and a comparison of RCs from different species will be presented.

RESULTS

The Primary Quinone. The primary quinone, Q_A, is located near the cytoplasmic side of the RC. Its position and orientation are well defined by the electron density, although there is no steric hindrance to moving the quinone to a position indicated by the dotted line in Fig. 1 (see below). The normal of the quinone ring forms an angle of ≈60° with respect to the membrane normal as defined by the direction of the twofold symmetry axis (4). Q_A interacts with the amino acid residues of the D, de, and E helices of the M subunit (3) (see Fig. 1).

The two carbonyl oxygens of Q_A are within hydrogen-bonding distance to the peptide nitrogen of Ala M260 and the side chain of Thr M222, respectively. Thr M222 also forms a hydrogen bond to the indole ring of Trp M252 (see purple dotted lines in Fig. 1). The distances between the hydrogens and the carbonyl oxygens were determined in *Rb. sphaeroides* from ENDOR experiments to be 1.55 Å and 1.78 Å (9). These are consistent with the distances observed in the structure. In *Rps. viridis*, the carbonyl oxygens of Q_A (menaquinone) were reported to form hydrogen bonds to a peptide nitrogen of Ala M258 (equivalent to M260 of *Rb. sphaeroides*) and the imidazole ring of His M217 (5) (equivalent to His M219 of *Rb. sphaeroides*). In *Rb. sphaeroides* the distance between the carbonyl oxygen of Q_A and His M219 is too large (4.5 Å) to form a hydrogen bond. However, an alternate sterically unhindered position of Q_A is possible, as shown by the dotted lines of Fig. 1; this position is within hydrogen-bonding distance of His M219.

Several aromatic residues that are located near Q_A, including Phe M251 and Trp M252, are conserved in all sequenced bacterial and plant systems. The aromatic ring of residue Trp M252 is approximately parallel to the quinone ring (the angle between ring normals is 25°). This residue bridges ϕ_A and Q_A; the distances of closest approach between its aromatic ring and ϕ_A and Q_A are 4.5 Å and 3.0 Å, respectively. The centers of the rings of Q_A, Trp M252, and Phe M251 lie approximately on a straight line. The normals of the aromatic rings of M252 and M251 form an angle of 75° and Trp M252 makes van der Waals contacts to both Q_A and M251. In addition, aromatic residues Phe M258 and Trp M268 are near Q_A. No ionizable residues other than the histidines liganded to Fe are located within 8 Å of the quinone ring, although two are found within 10 Å (Glu L104 near ϕ_A and Glu M234 near Fe).

The Secondary Quinone. The secondary quinone Q_B is also located near the cytoplasmic side of the RC with the normal of its ring forming an angle of ≈60° with respect to the membrane normal. Unlike for Q_A, the observed electron density for Q_B uniquely defines only the position of the quinone ring but not its orientation. An alternative orientation with the ring rotated by 180° about the isoprenoid chain is possible. However, consideration of hydrogen bonding favors the orientation shown in Fig. 2. The less well-defined electron density of the quinone ring may be due to either the presence of quinones in alternative orientations or motion of

The publication costs of this article were defrayed in part by page charge payment. This article must therefore be hereby marked "*advertisement*" in accordance with 18 U.S.C. §1734 solely to indicate this fact.

Abbreviations: RC, reaction center; D, bacteriochlorophyll dimer; ϕ, bacteriopheophytin; Q, quinone; subscripts A and B, branches A and B, respectively.

*This paper is no. 5 in a series. Papers 1, 2, 3, 4, and 6 are refs. 2, 3, 4, 7, and 8, respectively.

‡To whom reprint requests should be addressed.

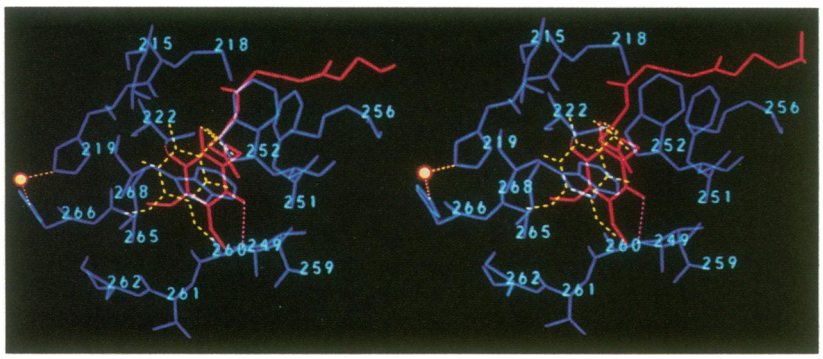

FIG. 1. Stereoview of primary quinone Q_A (red), Fe (small yellow sphere), and nearby residues of the M subunit (blue): Ala (249, 260), Asn 259, His (219, 266), Ile 265, Leu 215, Met (218, 256, 262), Phe 251, Thr (222, 261), Trp (252, 268). Hydrogen bonds are shown by dotted purple lines and Fe–His ligands are shown by dotted green lines. An alternative, sterically unhindered position of Q_A^- is shown by the dotted red lines. The twofold symmetry axis is approximately aligned in the paper with the cytoplasmic side at the bottom. The view is the same as in the figures of ref. 6 except it is rotated counterclockwise (as viewed from Fe to D) by ≈25° about the symmetry axis.

the quinone. Q_B interacts with the amino acid residues of the D, de, and E helices of the L subunit (see Fig. 2).

Two carbonyl oxygens of Q_B are within hydrogen-bonding distance to $N_{\delta 1}$ of His L190 (whose $N_{\epsilon 2}$ is liganded to Fe) and to the side chain of Ser L223. The residue Ser L223 is conserved in all bacterial and plant species and has been altered in several herbicide-resistant RC mutants (see *Discussion*). Based on the weak electron density of the sparsely populated Q_B site in *Rps. viridis*, similar hydrogen bonds were identified for the carbonyl oxygens of Q_B (6).

In contrast to Q_A, there are several ionizable residues located near Q_B; Glu L212 (conserved in all bacterial and plant systems that have been sequenced) and Asp L213 are in van der Waals contact with the quinone ring (see Fig. 2). In addition, residues Asp L210, Arg L217, Glu H173, and all five residues liganded to Fe are within 10 Å of the quinone ring. Arg L217 is positioned to form a salt bridge with Asp L210 or Asp L213.

Between ϕ_B and Q_B is the aromatic residue Phe L216 that is conserved in the bacterial and plant systems and is symmetry-related to Trp M252 near Q_A. The closest approach of the aromatic ring is 5 Å from ϕ_B and 4 Å from Q_B, with the ring normals of Phe L216 and Q_B forming an angle of 50°. The aromatic ring of Phe L216 does not make van der Waals contact with Q_B; this is in contrast to the configuration of Trp M252 near Q_A as discussed above.

The Nonheme Iron. The Fe^{2+} is located between Q_A and Q_B on the periplasmic side of the RC and is approximately positioned on the twofold symmetry axis relating the cofactors (2) (Fig. 3). The Fe is coordinated (see green dotted lines in Fig. 3) to the four $N_{\epsilon 2}$ atoms of His L190, L230, M219, and M266. These residues are located at the D and E helices and are conserved in all sequenced bacterial and plant systems. In addition, the de′ helix of M contributes the bidentate ligands of Glu M234 that is conserved only in bacterial species. A similar coordination was reported for *Rps. viridis* (5).

The Fe ligands form a distorted octahedron, in agreement with results obtained from a variety of spectroscopic measurements (10–13). The octahedral symmetry is formed by three axes; one between His L190 and His M219, a second between His L230 and His M266, and the third along Glu M234. The aromatic rings of His L190 and M219 lie approximately in a plane (the angle between the ring normals is ≈20°) and the line between the $N_{\epsilon 2}$ atoms passes through the iron. The aromatic rings of His L230 and M266 are also approximately parallel (the angle between ring normals is ≈20°), but the closest distance between the Fe and line between the $N_{\epsilon 2}$ atoms is ≈1.0 Å.

Two histidine rings, from residues L190 and M219, are located between the rings of Q_A and Q_B (Fig. 4). These histidines are part of a Q_B–His L190–Fe–His M219 system with Q_A close but beyond hydrogen-bonding distance to His M219. This arrangement suggests that the histidines play a role in the electron transfer from Q_A^- to Q_B.

DISCUSSION

Differences Between the Q_A and Q_B Sites. Several differences are observed between the Q_A and Q_B environments. The Q_A site is much more apolar than the Q_B site. The aromatic residue Trp M252 is in contact with Q_A, whereas no aromatic residues are in contact with Q_B. Several ionizable residues are near Q_B, in particular Glu L212 and Asp L213, whereas there are no charged residues near Q_A. The Fe is closer to Q_B by ≈2.0 Å. These factors contribute to the different functional properties of the quinones as discussed below.

Electron Transfer from Q_A^- to Q_B. *Stabilization of Q_B^- relative to Q_A^-.* Electron transfer proceeds vectorially from Q_A^- to Q_B, the free energy of Q_A Q_B^- being ≈70 meV lower than that of Q_A^- Q_B at pH 7 (14, 15). Since both quinones are UQ-10, the difference in energy must be due to different environments of the quinones. The following structural differences can contribute to the stabilization of the Q_A Q_B^- state. (*i*) There are more acidic residues in the vicinity of Q_B than Q_A. Although the presence of a negative charge on the carboxylic groups would raise the energy of Q_B^- (4), these

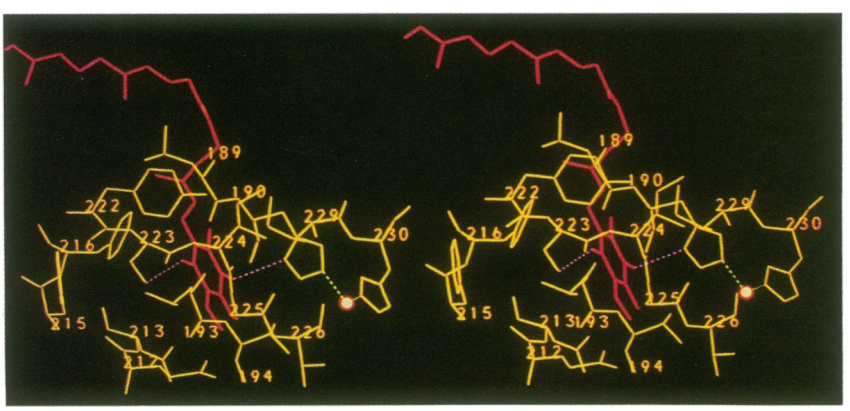

FIG. 2. Stereoview of secondary quinone Q_B (red), Fe (small yellow sphere), and nearby residues of the L subunit (yellow); Asp 213, Glu 212, Gly 225, His (190, 230), Ile (224, 229), Leu (189, 193), Phe (215, 216), Ser 223, Thr 226, Tyr 222, and Val 194. Hydrogen bonds are shown by dotted purple lines and Fe–His ligands are shown by dotted green lines. The view is the same as in figures of ref. 6.

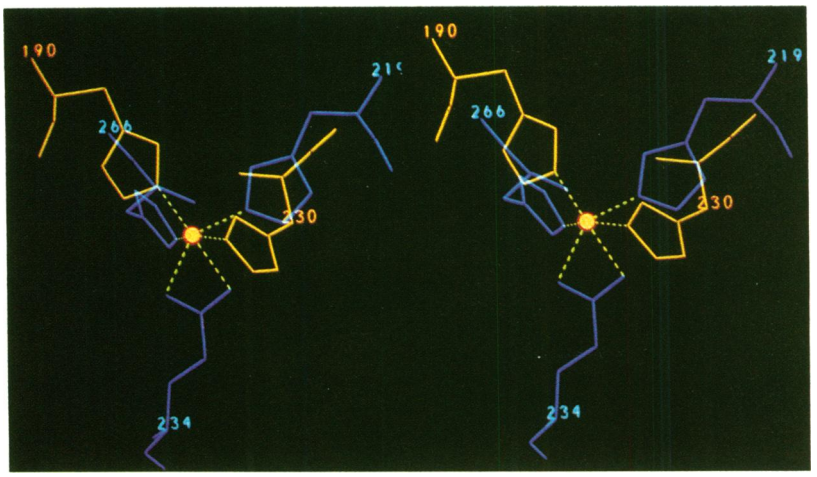

FIG. 3. Stereoview of iron atom Fe (small yellow sphere) and nearby residues (L subunit, yellow; M subunit, blue): His (L190, L230, M219, M266) and Glu M234. Fe–His and Fe–Glu ligands are shown by dotted green lines. The view is the same as in Fig. 2.

residues may be protonated, in which case their dipole interactions would lower the energy of Q_B^-. Residues that can be easily polarized would also lower the energy of Q_B^-. (*ii*) The Fe^{2+} is closer to the center of Q_B (8.5 Å) than to the center of Q_A (10.5 Å). As a consequence, the electrostatic potential due to the positive charge on the iron will lower the energy of Q_B^- relative to Q_A^-. A simple estimate that is based on the assumption of a single charge at the position of the iron results in a potential difference of 70 meV for a dielectric constant of 4.5. The Fe^{2+} in *Rps. viridis* is more symmetrically located between Q_A and Q_B [since both quinones are reported to form hydrogen bonds with histidines that ligand to the Fe (5, 6)]. For this system, the vectorial electron transfer from Q_A^- to Q_B may, in principle, be accounted for by the inherent difference between the redox potentials of menaquinone (Q_A) and ubiquinone (Q_B). The redox potential of menaquinone reconstituted in RCs from *Rb. sphaeroides*, measured by delayed fluorescence (16) was ≈20 meV lower than that of ubiquinone (P. McPherson and W. W. Parson, personal communication). Thus, in *Rps. viridis* the reduced effect of the electrostatic potential of Fe may be at least partially compensated for by the inherent difference in redox potentials of the quinones.

The presence of positively charged residues could stabilize the state $Q_AQ_B^-$ as compared to $Q_A^-Q_B$. However, there are no Arg or Lys residues within 7 Å of either quinone and the number of these residues, within a 20-Å sphere, is comparable for both quinones. This structural feature is therefore unlikely to contribute to the energy difference.

Activation energy of the electron transfer. The electron transfer rate from Q_A^- to Q_B has an activation energy of 560 meV (15). This large activation energy can be explained by the presence of polar residues in the Q_B binding site. According to the classical Marcus theory (17) the reorientation of the dipoles associated with these residues (e.g., the protonated residues Glu L212 and Asp L213) in the vicinity of Q_B^- will give rise to a reorganization energy λ that is much larger than the energy difference, δE, between the reactant (Q_A^- Q_B) and product (Q_A Q_B^-) states. This leads to an activation energy $\Delta E = (\delta E - \lambda)^2/4\lambda$.

The above argument can also be used to explain the observation that electron transfer from Q_A^- to Q_B is observed at cryogenic temperatures when RCs are frozen under illumination, whereas no electron transfer is observed when RCs are frozen in the dark (18). In the former case, the solvent reorganization around Q_B^- is stabilized in the product configuration (the dipoles are oriented), which makes the electron transfer essentially activationless.

Electrogenicity of the electron transfer from Q_A^- to Q_B and to Q_B^-. Electron transfers between cofactors of the RC are in general accompanied by a potential difference (i.e., an electrogenicity) across the membrane (19–22). An exception to this is the electron transfer from Q_A^- to Q_B (21, 23, 24). The lack of electrogenicity for this step can be explained by assuming that the electron path is parallel to the membrane surface. This is consistent with the structure, which shows that the line joining the centers of the quinones makes an angle of 85° ± 10° with the twofold symmetry axis of the RC—i.e., with the membrane normal (4).

The electron transfer of the second electron from Q_A^- to Q_B^- produces a small electrogenic potential (≈12% of the maximum produced by the D^+ Q_A^- charge separation) (23, 24). This can be explained either by a component of proton flow (toward Q_B^{2-}) parallel to the normal of the membrane or by a motion of the quinones relative to each other during the two-electron reduction.

The Charge Recombination Rates of Q_A^-, Q_B^- with D^+. Although the two quinones are approximately equidistant from the dimer (22 Å, edge to edge), the direct recombination rate of Q_B^- with D^+ is at least 2 orders of magnitude slower than that of Q_A^- with D^+ at 300 K (18). This may be explained by two possible mechanisms: (*i*) the direct recombination of Q_B^- with D^+ seems to be a thermally activated process (18), whereas that of Q_A^- is activationless. The difference is believed to be due to the presence of polar residues in the Q_B binding site as discussed before. (*ii*) The recombination proceeds via different protein pathways. This is formally described by a difference in the electron matrix element (overlap). Two general mechanisms have been postulated for this process (25–28). (*a*) In the "through space" mechanism, the electron path is assumed to be along the shortest line

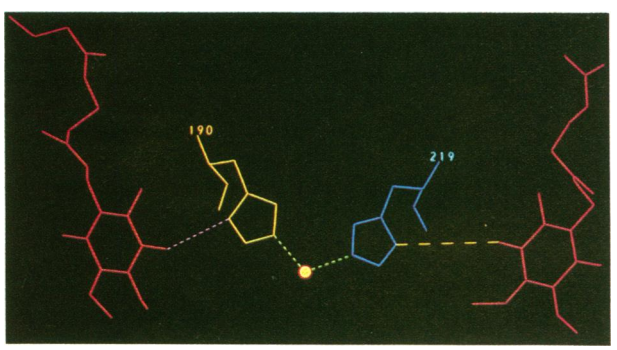

FIG. 4. The quinones, Q_A and Q_B (red), iron atom, Fe (small yellow sphere), His L190 (yellow), and His M219 (blue). A hydrogen bond is shown by a dotted purple line and Fe–His ligands are shown by dotted green lines. A yellow dashed line connects His M219 with Q_A. This view is approximately the same as in Fig. 2 except that it is rotated counterclockwise (as viewed from Fe to D) by ≈45° about the symmetry axis.

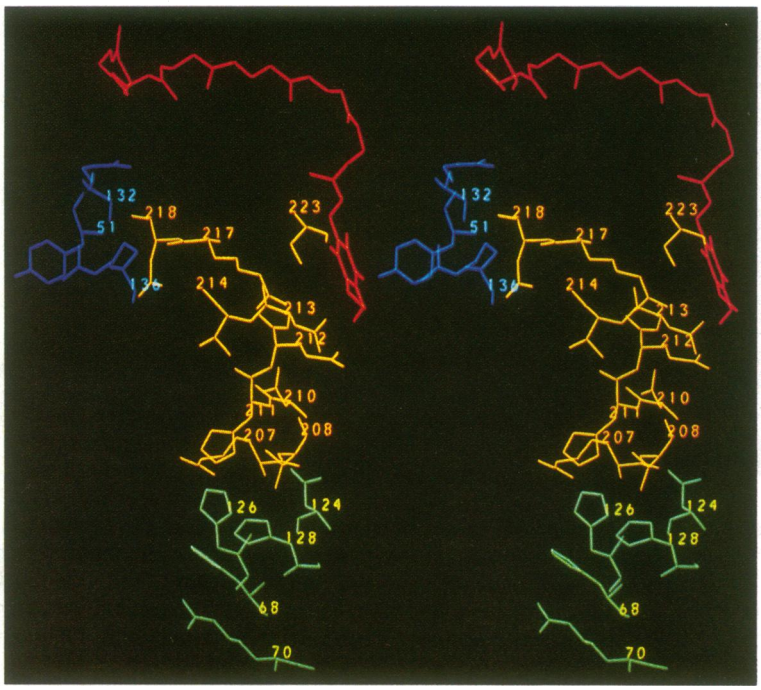

FIG. 5. Stereoview of secondary quinone, Q_B (red), and residues that may be involved in the pathway of protonation of Q_B (L subunit, yellow; M subunit, blue; H subunit, green): Arg (L207, L217, M132, M136, H70), Asp (L210, L213, L218, H124), Glu L212, His (L211, H68, H126, H128), Ser L223, Thr (L208, L214), and Tyr M51. This pathway may also involve solvent molecules in the interior of the RC; these, however, have not yet been incorporated into the analysis of the structure. The view is the same as in Fig. 2.

between donor and acceptor. More aromatic residues and fewer aliphatic residues are found between Q_A and D, than between Q_B and D; thus, the pathway from Q_A to D should be more favorable for electron transfer. (*b*) In the "through bond" mechanism, the electron path is assumed to be along chemical bonds. This mechanism involving the isoprenoid chains of the quinones is unlikely since the rate is independent of chain length (29). More likely is an electron pathway involving the D helices of the M and L subunits. The different charge recombination rates could then be due to the different bonding arrangements involving the residues of the D helices, the quinones, and the dimer.

Protonation of the Quinones and Exchange of Q_B H_2 with Exogenous Quinones. The transfer of electrons in the RC is accompanied by a transfer of protons. This is an essential function of the RC and forms the basis of the chemiosmotic hypothesis (30). The one-electron semiquinone species Q_A^- and Q_B^- are not protonated directly but interact with amino acid residues whose pK values are changed by electrostatic interactions, thus giving rise to the observed proton uptake (31, 32). When Q_B is doubly reduced, Q_B^{2-} accepts two protons and Q_B H_2 is replaced by an unprotonated, neutral exogenous, quinone. Two questions arise in connection with this process: (*i*) Can Q_B^{2-} be protonated inside the RC—i.e., how can exogenous protons enter the binding site? and (*ii*) How can Q_B H_2 (or Q_B^{2-}) leave the RC?

Equilibration of exogenous protons with the interior of the RC. If Q_B^{2-} is protonated inside the RC, the exogenous protons can enter, in principle, via two mechanisms: In one, a channel connects Q_B to the surface of the RC exposing it to the outside solvent. An examination of the RC structure revealed no such channels. Alternatively, protonation can occur through a "bucket brigade." In this mechanism, protons are transferred from the surface to Q_B through a chain of protonatable residues, the last one being exposed to the solvent. In Fig. 5 we show protonatable residues in the vicinity of the Q_B site. Two chains of residues that can form proton bridges to the surface are discernible. It should be noted that the problem of proton accessibility is not unique to the Q_B^{2-} problem; proton uptake (release) that is associated with the reduction of ϕ_A, Q_A, Q_B, and the oxidation of D poses the same problem.

How does Q_B H_2 (or Q_B^{2-}) leave the RC? By a Monte Carlo calculation, the quinone ring was repositioned throughout the RC along the isoprenoid chain, and the van der Waals contacts with the protein environment were determined. The channel formed inside the RC protein by the isoprenoid chain was found to be everywhere large enough for the quinone ring to pass without requiring structural changes. Thus, the isoprenoid chain may "pave" the way for the exit of the quinone. In contrast to Q_B, a similar analysis demonstrated that Q_A cannot dissociate from the RC without changes in the RC structure. In Fig. 6, we show the van der Waals surface of Q_B including its isoprenoid chain. The ring of Q_B and the proximal section of its isoprenoid chain are buried inside the RC. The distal part of the isoprenoid chain lies near the surface of the RC close to the cytoplasmic side of the lipid bilayer (4). There are two possible mechanisms for quinone release. In one, the Q_BH_2 state is formed inside the RC. Q_BH_2 may form different hydrogen bonds to the RC, which would lower its binding affinity. Alternatively, Q_B^{2-} may be released to the surface of the RC before it is protonated. In this case, release may be facilitated by electrostatic forces that open the structure.

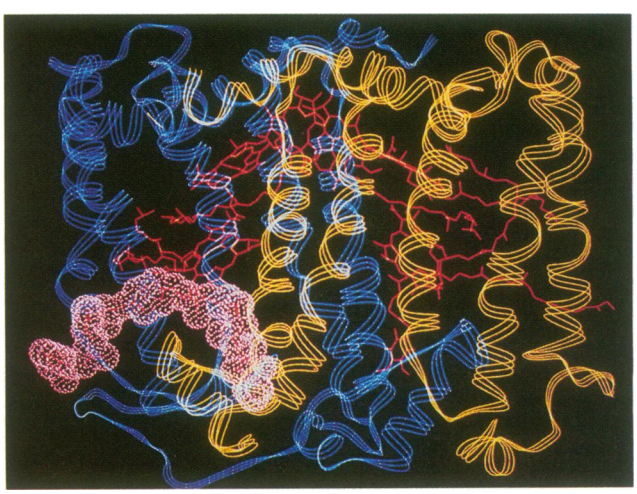

FIG. 6. Backbones of the L subunit (yellow), M subunit (blue), and cofactors (red). The van der Waals surface of Q_B (dotted pink) that outlines a possible pathway for Q_B to leave the RC is shown (see text). The view is the same as in Fig. 1.

Both Q_A and Q_B can be removed in the presence of *o*-phenanthroline and a high concentration of detergent (33). Presumably the detergent opens up the structure and the *o*-phenanthroline competes successfully with the quinones for the binding site.

Herbicide-Resistant Mutants. Electron transfer from Q_A^- to Q_B in bacterial RCs is inhibited by triazine herbicides. The mode of action of herbicides is believed to be competition with the quinone for the binding site (34). Herbicides have been found to bind in RCs from *Rps. viridis* (5) in the region that is homologous to the Q_B binding site of *Rb. sphaeroides*. Three mutants of *Rb. sphaeroides* that are resistant to herbicides have been isolated and sequenced (35–37). All mutations occur on the L subunit; they are Ile 229 → Met; Ser 223 → Pro and Tyr 222 → G. All mutants show a greatly reduced binding affinity for Q_B (37). This can be understood from an inspection of the structure (Fig. 2). Ser 223 is hydrogen bonded to Q_B; the mutation to Pro eliminates this hydrogen bond and should, in addition, cause conformational changes at the site. Ile 229 is in close contact with the ring of Q_B; the mutation to the unbranched larger residue, Met, may reduce Q_B binding due to steric interference. Tyr 222 is not in contact with Q_B but forms a hydrogen bond with the backbone of the M subunit (Leu M39 and Asn M44). The effect of the Tyr → Gly mutation is to break this hydrogen bond; this apparently causes a conformational change that results in a reduced binding constant of Q_B (37). The binding constant of the herbicide in these mutants is reduced to a greater extent than that of the quinone. A more detailed understanding of this awaits the determination of the structures of the herbicide–RC complex and the mutant RCs.

All the residues involved in the mutations discussed above are conserved between the purple bacterial species. This suggests the importance of these residues for the functioning of the RC and is consistent with the reduced photosynthetic efficiencies (due to reduced quinone binding and reduced electron transfer rates) of the mutants (37).

Comparison of the Fe^{2+} in the RC with Metals in Other Proteins. The Fe^{2+} in the RC is bound at the interface of the L and M subunits where it may stabilize their tertiary structure. A similar location of a nonheme Fe at the interface of two homologous subunits has recently been reported in protocatechuate 3,4-dioxygenase.[¶] The coordination of Fe^{2+} by histidines and carboxyl side chains is typical of the binding interactions of many transition metals to proteins (for a review, see ref. 38). Well-characterized examples of such proteins are the superoxide dismutases, which contain different divalent metals, and carboxypeptidase A, which contains Zn. The iron in the RC does not change oxidation state during charge separation. The metals of some of the other proteins, such as the Fe in superoxide dismutase, change valence during enzymatic activity.

The removal of the Fe from the RC alters, but does not eliminate, activity. In contrast, when the metals of other proteins, such as superoxide dismutase and carboxypeptidase A, are removed, activity is lost.

RCs can be reconstituted with Fe or with a variety of other divalent metal ions (i.e., Zn, Ni, Co, Mn, Cu) and exhibit electron-transfer characteristics that are essentially undistinguishable from native RCs (39). This suggests that the charge on the metal ion rather than the detailed electronic structure of the ion is important for restoring the native function of the RC.

[¶]Ohlendorf, D. H., Weber, P. C. & Lipscomb, J. D., American Crystallographic Association Meeting, June 26–July 1, 1988, Philadelphia, **16**, 70 (abstr.).

We thank E. Abresch for preparation of the RCs and M. Y. Okamura, W. Lubitz, and A. Chirino for helpful discussions. This work was supported by grants from the National Institutes of Health (AM36053, GM13191, GM31875) and the National Science Foundation (DMB85-18922 and a Presidential Young Investigators Award). D.C.R. is an A. P. Sloan research fellow.

1. Okamura, M. Y., Feher, G. & Nelson, N. (1982) in *Photosynthesis*, ed. Govindjee (Academic, New York), pp. 195–272.
2. Allen, J. P., Feher, G., Yeates, T. O., Komiya, H. & Rees, D. C. (1987) *Proc. Natl. Acad. Sci. USA* **84**, 5730–5734.
3. Allen, J. P., Feher, G., Yeates, T. O., Komiya, H. & Rees, D. C. (1987) *Proc. Natl. Acad. Sci. USA* **84**, 6162–6166.
4. Yeates, T. O., Komiya, H., Rees, D. C., Allen, J. P. & Feher, G. (1987) *Proc. Natl. Acad. Sci. USA* **84**, 6438–6442.
5. Michel, H., Epp, O. & Deisenhofer, J. (1986) *EMBO J.* **5**, 2445–2451.
6. Michel, H. & Deisenhofer, J. (1988) *Biochemistry* **27**, 1–7.
7. Yeates, T. O., Komiya, H., Chirino, A., Rees, D. C., Allen, J. P. & Feher, G. (1988) *Proc. Natl. Acad. Sci. USA* **85**, 7993–7997.
8. Komiya, H., Yeates, T. O., Rees, D. C., Allen, J. P. & Feher, G. (1988) *Proc. Natl. Acad. Sci. USA*, in press.
9. Feher, G., Isaacson, R. A., Okamura, M. Y. & Lubitz, W. (1985) in *Antennas and Reaction Centers of Photosynthetic Bacteria*, ed. Michel-Beyerle, M. E. (Springer, Berlin), pp. 174–189.
10. Boso, B., Debrunner, P., Okamura, M. Y. & Feher, G. (1981) *Biochim. Biophys. Acta* **638**, 173–177.
11. Bunker, G., Stern, E. A., Blankenship, R. E. & Parson, W. W. (1982) *Biophys. J.* **37**, 539–551.
12. Eisenberger, P., Okamura, M. Y. & Feher, G. (1982) *Biophys. J.* **37**, 523–538.
13. Butler, W. F., Calvo, R., Fredkin, D. R., Isaacson, R. A., Okamura, M. Y. & Feher, G. (1984) *Biophys. J.* **45**, 947–973.
14. Mancino, L. J., Dean, D. P. & Blankenship, R. E. (1984) *Biochim. Biophys. Acta* **764**, 46–54.
15. Kleinfeld, D., Okamura, M. Y. & Feher, G. (1984) *Biochim. Biophys. Acta* **766**, 126–140.
16. Woodbury, N. W., Parson, W. W., Gunner, M. R., Prince, R. C. & Dutton, P. L. (1986) *Biochim. Biophys. Acta* **851**, 6–22.
17. Marcus, R. A. (1956) *J. Chem. Phys.* **24**, 966–978.
18. Kleinfeld, D., Okamura, M. Y. & Feher, G. (1984) *Biochemistry* **23**, 5780–5786.
19. Schönfeld, M., Montal, M. & Feher, G. (1979) *Proc. Natl. Acad. Sci. USA* **76**, 6351–6355.
20. Packham, N. K., Packham, C., Mueller, P., Tiede, D. M. & Dutton, P. L. (1980) *FEBS Lett.* **110**, 101–106.
21. Packham, N. K., Dutton, P. L. & Mueller, P. (1982) *Biophys. J.* **37**, 465–473.
22. Trissl, H. W. (1983) *Proc. Natl. Acad. Sci. USA* **80**, 7173–7177.
23. Feher, G. & Okamura, M. Y. (1984) in *Advances in Photosynthesis Research*, ed. Sybesma, C. (Nijhoff/Junk, The Hague, The Netherlands), Vol. 2, pp. 155–164.
24. Kaminskaya, O. P., Drachev, L. A., Konstantinov, A. A., Semenov, A. Y. & Skulachev, V. P. (1986) *FEBS Lett.* **202**, 224–228.
25. Mayo, S. L., Ellis, W. R., Jr., Crutchley, R. J. & Gray, H. B. (1986) *Science* **233**, 948–952.
26. Kuki, A. & Wolynes, P. G. (1987) *Science* **236**, 1647–1652.
27. Closs, G. L. & Miller, J. R. (1988) *Science* **240**, 440–447.
28. Sneddon, S. F., Morgan, R. S. & Brooks, C. L. (1988) *Biophys. J.* **53**, 83–89.
29. Gunner, M. R., Robertson, D. E. & Dutton, P. L. (1986) *J. Phys. Chem.* **90**, 3783–3795.
30. Mitchell, P. (1968) in *Chemiosmatic Coupling and Energy Transduction* (Glynn Research, Bodmin, Cornwall, U.K.).
31. Maroti, P. & Wraight, C. A. (1988) *Biochim. Biophys. Acta* **934**, 329–347.
32. McPherson, P. H., Okamura, M. Y. & Feher, G. (1988) *Biochim. Biophys. Acta* **934**, 348–368.
33. Okamura, M. Y., Isaacson, R. A. & Feher, G. (1975) *Proc. Natl. Acad. Sci. USA* **72**, 3491–3495.
34. Wraight, C. A. (1981) *Isr. J. Chem.* **21**, 348–354.
35. Gilbert, C. W., Williams, J. G. K., Williams, K. A. L. & Arntzen, C. J. (1985) in *Molecular Biology of the Photosynthetic Apparatus*, eds. Steinback, K. E., Bonitz, S., Arntzen, C. J. & Bogorad, L. (Cold Spring Harbor Lab., Cold Spring Harbor, NY), pp. 67–71.
36. Schenck, C. C. (1986) *Biophys. J.* **49**, 486a (abstr.).
37. Paddock, M. L., Rongey, S. H., Abresch, E. C., Feher, G. & Okamura, M. Y. (1988) *Photosynth. Res.* **17**, 75–96.
38. Harrison, P. M., ed. (1985) *Metalloproteins* (Verlag Chemie, Berlin).
39. Debus, R. J., Feher, G. & Okamura, M. Y. (1986) *Biochemistry* **25**, 2276–2287.